Molecular Theory of the Sphere-to-Rod Transition and the Second CMC in Aqueous Micellar Solutions

Sylvio May[†] and Avinoam Ben-Shaul*[,‡]

Institut für Biochemie und Biophysik, Friedrich-Schiller-Universität Jena, Philosophenweg 12, 07743 Jena, Germany, and Department of Physical Chemistry and the Fritz Haber Research Center, The Hebrew University, Jerusalem 91904, Israel

Received: August 22, 2000; In Final Form: October 30, 2000

We present a molecular-level theory for amphiphile packing in linear micelles, focusing on the early stages of micellar elongation, i.e., on small and "intermediate-size" micelles, whose endcaps are not yet molded into a final shape. The internal free energy of a micelle of given size and shape is expressed as an integral over local molecular packing free energies in different regions of the micelle. The free energy per molecule is expressed as a sum of interfacial ("opposing forces") and chain conformational contributions, both depending on the local geometry. The equilibrium shape and energy of the micelle is determined by functional minimization of the total free energy. For amphiphiles exhibiting strong preference for packing in the cylindrical geometry, we show that the early stages of growth involve an energetic barrier, resulting in a "gap" in the micellar size distribution. That is, at low total amphiphile concentrations only small (globular) micelles appear in solution. Their concentration reaches a well-defined saturation value, beyond which, all added amphiphiles are incorporated in long micelles, whose "non-interacting" endcaps are well separated by the cylindrical middle part. This, "second CMC" behavior is demonstrated by numerical calculations of micellar size distributions and average aggregation numbers as a function of the total concentration. The conditions necessary for the appearance of a second CMC are analyzed theoretically, with explicit reference to the underlying molecular packing characteristics. In particular, it is shown that a necessary condition for the appearance of a sharply defined second CMC is that the endcap energies (of at least some) of the small or intermediate-size micelles must be considerably lower than the asymptotic (long micelle) value of this quantity. The diameter of the minimal, spherical micelles, as well as that of the final endcaps, is found to be larger than the diameter of the cylindrical body of the very long micelles. Our results are in good qualitative agreement with recent cryo-TEM imaging studies of micellar shape and growth, as well as with previous (less direct) experiments revealing second CMC behavior.

Introduction

Linear, rodlike, micelles are often modeled as spherocylinders.[1−5] That is, the micelle is assumed to consist of a cylindrical body, capped by two hemispherical ends whose radius is equal to that of the cylindrical middle part. This is the "standard" structural model for both rigid (rodlike) and flexible, ("worm-like") micelles. On the basis of this model, the internal packing free energy (the standard chemical potential) of a linear micelle composed of N amphiphilic molecules can be expressed in the simple form

$$\mu^0(N) = Nf(N) = (N - M)f^{cyl} + M f^{sph} = N f^{cyl} + 2\delta \; (N \geq M) \tag{1}$$

where M is the number of amphiphiles constituting the minimal, namely spherical, micelle. Pictorially, this model suggests that micellar growth ($N > M$) takes place by "splitting" a spherical micelle into two hemispheres, each containing $M/2$ molecules, with the added, $N - M$, molecules forming the cylindrical middle part; f^{cyl} and f^{sph} denote the molecular packing energies in the cylindrical and spherical regions, respectively, and $\delta = (M/2)(f^{sph} - f^{cyl})$ is the excess energy of the endcap relative to the cylindrical body. Because, entropically, partitioning a given number of amphiphiles into small micelles is preferable over their packing in longer micelles, it is clear that micellar growth (with increasing total concentration) can only take place if $\delta > 0$. (Note that 2δ is also the energetic cost of breaking a long micelle into two shorter ones.)

The consequences of the spherocylinder model and eq 1 with respect to micellar growth ("the sphere-to-rod" transition) in dilute solution are well-known.[6−8] In particular, this model predicts that the growth process is *continuous*. That is, the average micelle size, $\langle N \rangle$, increases monotonically with the total mole fraction of amphiphile in solution, X. At, and just above, the critical micellar concentration (CMC, X_c), $\langle N \rangle \approx M$. Well above the CMC, i.e., when $\langle N \rangle \gg M$, the weight average aggregation number increases with concentration according to the familiar growth law

$$\langle N \rangle = 2\sqrt{X} \exp(\delta) \tag{2}$$

It is also known that the micellar size distribution is polydis-

* To whom correspondence should be addressed. Tel: 972-2-6585271. Fax: 972-2-6513742. E-mail: abs@fh.huji.ac.il.

[†] Institut für Biochemie und Biophysik, Friedrich-Schiller-Universität Jena. Tel: 49 3641 9 49393. Fax: 49 3641 9 49352. E-mail: may@avalon.biologie.uni-jena.de.

[‡] Department of Physical Chemistry and the Fritz Haber Research Center, The Hebrew University.

10.1021/jp003021o CCC: $20.00
Published on Web 12/29/2000

perse,[6] of width $\Delta N = [\langle N^2\rangle - \langle N\rangle^2]^{1/2} \sim \langle N\rangle$. It should be noted that in eq 2 and throughout this paper all energies, (e.g., δ, f and μ^0) are measured in units of k_BT, where k_B is Boltzmann's constant, and T the is temperature.

Depicting the endcaps of a linear micelle as perfect hemispheres, exactly matching the cylinder's cross section, is certainly an approximation. In fact, simple molecular packing considerations[7−9] (see the discussion in the next section) and computer simulations[10] suggest that the radius of a minimal, spherical micelle (b_s) is larger than the radius of the cylindrical body of a long micelle, (b_c). Regardless of the specific structure and energy of the endcaps it is clear that all "long-enough" micelles consist of a cylindrical mid-section and two well-defined endcaps. Clearly, however, if the final shape of these endcaps is not a simple hemisphere, then there must be a finite range of "intermediate-size" micelles, $M < N < L$, whose structure is neither spherical nor that of a cylinder capped by two "non-interacting" endcaps. Later in this paper, we shall see that L may be as high as $\sim 3M$.

Although the spherocylinder model is not always applicable, the last expression in eq 1 is valid for the long micelle population ($N > L$). (In fact, this expression and the ensuing growth law, eq 2, apply to all kinds of one-dimensional (1D) growth processes; e.g., the distribution of cluster sizes of an interacting 1D lattice gas.[6]) Thus, well above the CMC, when most amphiphiles are incorporated in long micelles, their general growth characteristics are similar to those predicted by the spherocylinder model, with δ representing their endcap energy. In particular, the size distribution of the long micelle population will be polydisperse and their average micellar size increases with total concentration according to eq 2.

On the other hand, eq 1 may fail in describing the packing free energy of the intermediate-size micelles ($M < N < L$). Deviations from the simple spherocylinder model may be reflected in rather unexpected growth behaviors of micellar sizes.[11−16] Some 15 years ago, on the basis of magnetic birefringence and viscosity measurements of cetylpyridinium bromide (CPBr) micelles, Porte et al.[11] observed a rather peculiar growth behavior of these micelles. Namely, micellar growth was found to take place in two well-defined stages. In the first stage, corresponding to the concentration regime $X_c \le X \le X_{2c}$ (X_c denoting the constant, free monomer, concentration at the CMC), all added ($X - X_c$) amphiphiles are aggregated in small micelles, of sizes $N \approx M$. This behavior prevails until X reaches another critical value, X_{2c}, marking the transition into the second stage of growth. Namely, once X exceeds X_{2c} the concentration of small micelles saturates, i.e., remains equal to X_{2c}, while all added amphiphiles begin organizing into long micelles of size $N > L$, showing the expected growth behavior of linear micelles, eq 2. This transition from a saturated solution of small micelles to a solution containing long and growing micelles, coexisting with the smaller ones, is reminiscent of the behavior at the ordinary CMC, where the concentration of free monomers saturates and the added monomers are involved in micelle formation. Consequently, the second transition, from short to long micelles, has been termed[11] the "second CMC", with X_{2c} denoting the total amphiphile concentration at this point. It should be noted that the concentration of intermediate-size micelles was very small at all concentrations, indicating a "gap" in the size distribution of the micelles.

The absence of certain (or all of the) micelles of intermediate size is a clear indication that the average molecular packing energies in these micelles, f, are significantly higher than those in both smaller and larger micelles. On the basis of this notion, Porte et al.[11] have suggested a phenomenological structural model for linear micelles, which could account for the second-CMC behavior observed in their experiments on CPBr solutions. Other groups have reported similar experimental results for different micellar systems, and proposed alternative, albeit similar, phenomenological models for their interpretation. In particular, Kato et al.[13] have examined several possible phenomenological models for $\mu^0(N)$, to explain the second-CMC behavior observed in their light scattering investigation of nonionic ($C_{12}E_5$) micelles. Only one of the proposed models, involving different values for the endcap energy (δ) of intermediate-size and long micelles, could account for their observations.

A most direct demonstration of a second-CMC has recently been reported by Bernheim-Groswasser et al. for micellar solutions of both cationic dimeric[12] (gemini) and nonionic[17] surfactants. Using cryo-TEM microscopy, these authors have shown that the growth of these micelles is characterized by two distinct stages, and two distinct micellar populations. At very small concentrations (yet well above the main CMC), all of the micelles are small and globular. At higher concentration, above the second CMC, these small micelles coexist with much longer (semiflexible) linear micelles. Furthermore, the cryo-TEM micrographs show very clearly that the diameter of the small micelles, as well as of the micellar endcaps, are distinctly larger than the diameter of the cylindrical bodies of the long micelles. Another very clear visualization of the micellar end cap thickening was recently reported by Zheng et al.[18] for the case of diblock copolymers.

Motivated by these new experiments, we here present a *molecular-level* theory for the structure and growth of linear micelles, taking into account all the relevant (headgroup, surface, and tail) contributions to the packing free energies of amphiphiles in micelles of all sizes N. We focus on analyzing the structure of intermediate-size micelles, and show that a barrier in the packing free energy profile is indeed possible, and that the endcaps can be significantly bulkier than the cylindrical body. Our structural-energetic model is presented in the next section. Later in this paper, we shall use the calculated free energies to derive micellar size distributions, showing very clearly that the appearance of a well defined second CMC reflects, in a rather direct fashion, the packing characteristics of the constituent amphiphiles. Finally, in discussing the results, we reiterate, using our terminology, the conditions necessary for observing a second-CMC behavior. It should be stressed that our theoretical treatment is limited to the dilute solution regime, where intermicellar interactions do not affect the size and shape of the micelles or their size distribution. Also, elongated micelles are assumed to be perfectly linear, thus ignoring higher order effects such as micellar flexibility and branching. Whenever present, these effects are manifsted at rather high surfactant concentrations, significantly higher than the second CMC.

Theory

Consider an aqueous micellar solution in which the total mole fraction of amphiphile is $X_{tot} = X(1) + X$, where $X(1)$ is the mole fraction of free monomers, and X is the overall mole fraction of micellized amphiphile. Here, we are interested in the micellar growth process (rather than the association of monomeric amphiphiles into micelles) which takes place at $X \ge X_c$ where X_c is the CMC. Above the CMC $X(1) \approx X_c$ is essentially constant, implying that an increase in X_{tot} is only reflected in X. Thus, we can safely ignore the role of monomeric

amphiphiles and refer to X as the total mole fraction of (micellized) amphiphiles.

Assuming that the smallest aggregate in solution is a spherical micelle containing M amphiphiles we can write,

$$X = \sum_{N \geq M} X(N) \approx \int_M^\infty X(N)dN \tag{3}$$

where $X(N)$ is the mole fraction of amphiphiles packed in micelles of size N. Note that the concentration of "N-micelles" is proportional to $X(N)/N$. Replacing the sum by an integral is, of course, an excellent approximation for all concentrations above the CMC.

In dilute solutions, intermicellar interactions can be neglected, and the Helmholtz free energy of the system (in units of k_BT) is given by

$$F = C \int_M^\infty dN \left[\frac{X(N)}{N}\mu^0(N) + \frac{X(N)}{N}\left(\ln \frac{X(N)}{N} - 1\right)\right] \tag{4}$$

where $\mu^0(N) = Nf(N)$ is the standard chemical potential of an N-micelle, and $f(N)$ is the average packing energy per molecule in the micelle. The constant C relates $X(N)/N$ to the number of N-micelles in solution, $n(N)$; namely, $C = n(N)/[X(N)/N] \approx V_{tot}/\nu_w$, where V_{tot} is the total volume of the solution and ν_w is the volume of a solvent molecule. Note that

$$\mu^0(N) + \ln[X(N)/N] = \mu(N) \tag{5}$$

is the chemical potential of N-micelles, with the first term representing their packing free energy and the second term accounts for their translational ("mixing") entropy. The last term in eq 4 is the contribution of N-micelles to the osmotic pressure, Π, consistent with the thermodynamic relation $F = G - \Pi V_{tot} = \Sigma_N\, n(N)\mu(N) - \Pi V_{tot}$, where G is the Gibbs free energy of the system.

The equilibrium distribution of micellar sizes is determined by minimizing F with respect to $\{X(N)\}$, subject to the conservation condition, eq 3. This minimization yields the familiar expression

$$X(N) = N \exp[-(\mu^0(N) - N\mu)] \tag{6}$$

The quantity $\mu = \mu(X,T)$ appearing in this equation is the Lagrange multiplier conjugate to the material conservation constraint, eq 3. Of course,

$$\mu = \mu(N)/N = \text{constant} \tag{7}$$

is the chemical potential per amphiphile in solution, which must be the same everywhere in the system, i.e., in all N-micelles, as well as in the monomeric form, $N = 1$. Because $\mu = \mu(1) = \mu^0(1) + \ln[X(1)]$, eq 6 can also be expressed in the well-known alternative form $X(N) = N\, X(1)^N \exp[-(\mu^0(N) - N\mu^0(1))]$.[8]

Any deviation of the micelle size distribution and the growth behavior from those predicted by the spherocylinder model must be reflected in a corresponding deviation of $\mu^0(N)$ from the simple phenomenological expression eq 1. Our goal in the following sections is to present a molecular-level model for $\mu^0(N)$, explaining the molecular origin of such deviations.

2.1 Molecular Model. In eq 1, the internal (packing) free energy of a spherocylindrical micelle has been expressed as the weighted sum of the molecular free energies in the cylindrical and spherical geometries, assuming that all molecules in each of these two environments are equivalent. More generally, the internal free energy of an (arbitrarily shaped) N-micelle is a sum of the local molecular free energies, f, corresponding to the the various microenviroments in the micelle. In integral form, $\mu^0(N) = \int dNf$, where the integration is over all molecules in the various local geometries of the micelle. The optimal shape of the micelle can be determined by functional minimization of $\mu^0(N)$, i.e., by minimizing this integral with respect to all possible aggregation geometries. In the next section, we shall apply this procedure for deriving the equilibrium shape and energy of linear micelles, for all $N \geq M$. To this end, we first need an explicit expression for the local packing free energy, f. Our model for f, though simple, accounts for all the important characteristics of amphiphile packing in micellar aggregates.

Quite generally, the packing free energy per molecule can be expressed as a sum of two contributions

$$f = f_o + f_t \tag{8}$$

where the first, "interfacial", term accounts for intermolecular interactions in the headgroup region of the micelle, and the second term represents the internal free energy of the hydrophobic tail. Both terms depend on the local packing geometry.

For f_o, we shall use the familiar "opposing forces" model (OFM), which expresses the interfacial energy as a sum of a repulsive term accounting for headgroup−headgroup interactions and an attractive contribution associated with the interfacial energy between the (surface of the) hydrophobic core and the surrounding aqueous solvent.[7,8] A simple, often used, representation of this model is $f_o = B/a + \gamma a$, with a denoting the local area per molecule at the hydrocarbon−water interface, B is a molecular constant measuring the strength of inter-headgroup repulsion (due to excluded volume, or electrostatic interactions, or both), and γ is the effective surface tension between the hydrophobic and aqueous regions. Clearly, the first term tends to maximize a, whereas the second tends to minimize it. Using $a = a_o = (B/\gamma)^{1/2}$ to denote the value of a at which these opposing forces balance each other (i.e., minimize f_o), and neglecting irrelevant constant terms, one can express f_o in the equivalent form

$$f_o = \gamma a \left(1 - \frac{a_o}{a}\right)^2 \tag{9}$$

The hydrophobic tail of an amphiphile is a flexible chain, possessing many possible conformations. The conformational entropy of such chains is largely reduced upon their packing within the dense hydrophobic core of a micellar aggregate. The extent of the change in chain conformational entropy (as well as in chain energy, and hence, in free energy) depends on the packing geometry, e.g., spherical versus cylindrical.[6] On the basis of detailed, molecular-level calculations of such free energy variations, an approximate simple representation of f_t in different local packing geometries is provided by the quadratic expression[19,20]

$$f_t = \tau(b - b^*)^2 \tag{10}$$

Here, b is the radius of the (hydrophobic core of the) micelle in question, e.g., spherical or cylindrical, b^* is its optimal value, and τ is an elastic stretching modulus, related to the conformational flexibility of the chains. In general, both τ and b^* depend on the aggregation geometry. Note also that b^* cannot exceed the maximal, *all-trans*, chain length l because this would

imply the intolerable free-energy penalty associated with creating a void in the center of the hydrophobic core.

Detailed molecular calculations for micelles composed of 14-carbon (C-14) tails reveal that τ is essentially the same for spherical and cylindrical micelles.[19] However, the corresponding b^*'s are different. Specifically, it was found that $b^*(\mathrm{sph}) = l$, whereas $b^*(\mathrm{cyl}) \approx 0.8l$. Qualitatively, this difference arises from the fact that in a spherical micelle, only a very small fraction of the chains are "stretched to the limit" (because the available volume in a sphere decreases quadratically with the distance from the interface), whereas most chains are relaxed and enjoy nearly maximal conformational freedom. By contrast, in a cylindrical micelle, the available volume decreases only linearly with the distance from the interface, implying that a larger fraction of the chains must be fully stretched when $b = l$. Consequently, maximal chain conformational freedom is reached for $b^*(\mathrm{cyl}) < b^*(\mathrm{sph}) = l$. These conclusions are not limited to C-14 chains.

On the basis of the assumption that the hydrophobic core of micellar aggregates is uniformly dense and incompressible, simple relationships can be derived between a, the area per molecule at the core surface, and the core radius, b. In particular, for perfect spheres, cylinders and planar bilayers (where b refers to their half-thickness) one finds $a = i\nu/b$, with $i = 3$, 2, and 1 for these three geometries, respectively; ν denotes the chain's volume. Because b cannot exceed the length of the fully extended amphiphile tail, l, this implies that $a \geq i\nu/l$. The preferred aggregation geometry in solution can now be predicted based on two simple physical principles.[7,8] First, amphiphiles will only pack in aggregates enabling $a = a_e$ (equivalently $b = b_e$), where a_e is the optimal (interfacial) area per headgroup, corresponding to the minimum of f. Second, the thermodynamically preferred aggregation geometry is the smallest micelle allowing $a = a_e$. This is because partitioning a given number of amphiphiles into many small aggregates is entropically more favorable than arranging them into fewer larger aggregates.

These useful notions are conveniently cast in terms of the *packing parameter*, $p \equiv a_e l/\nu$. Considering the three perfect geometries mentioned above, we conclude that spherical micelles will prevail in solution if $p \geq 3$, cylindrical micelles are the preferred aggregation geometry when $3 > p \geq 2$, and bilayers are formed when $2 > p \geq 1$.

In general, the optimal molecular parameters, a_o,b_o, predicted by the minimum of the OFM (interface) free energy f_o, are different from those, a^*,b^*, which minimize the tail free energy, f_t. In other words, neither of those predictions exactly agree with a_e,b_e, whose value is determined by simultaneous minimization of $f = f_o + f_t$. Recall, however, that according to the OFM scheme the optimal radius of a cylindrical micelle is given by $b_o = 2\nu/a_o = 2l/y$, where $y \equiv a_o l/\nu$ is the value of the packing parameter in the OFM approximation, ($a_e = a_o$). Because $b^*(\mathrm{cyl}) < l$, there must be a particular value y ($3 > y > 2$) for which $b_e = b_o = b^*(\mathrm{cyl})$, (hence $y = p$). For this (and around this) particular value of y, the cylindrical micelle provides the optimal packing geometry for *both* the headgroups and the tails. By contrast, because $y < 3$, it follows that amphiphile packing in a spherical environment must involve a nonzero free energy penalty. The lowest penalty possible corresponds to a spherical micelle of maximal radius $b_s = b^*(\mathrm{sph}) = l = (y/2)b_c > b_c = b_o = b^*(\mathrm{cyl})$. Thus, amphiphiles with such molecular (y) characteristics will preferentially pack into elongated, "cylindrical", micelles. Furthermore, the endcaps of these micelles are expected to be bulkier than their cylindrical body. Our explicit calculations of micellar shapes, energies, and size distributions will focus on micelles showing this behavior. It should be stressed that our theoretical treatment is limited to the dilute solution regime, where intermicellar interactions do not affect the micelle size distribution. Furthermore, the elongated micelles are assumed to be perfectly linear, thus ignoring the effects of micellar flexibility and branching.

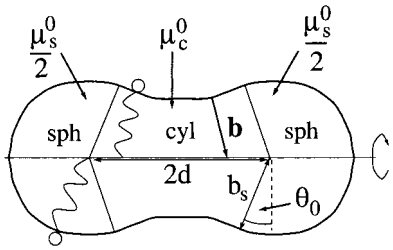

Figure 1. Schematic illustration of a rodlike micelle. Shown is a cross section through its hydrophobic interior. The two spherical endcaps (of radius b_s) are separated by a cylindrical middle part (of length $2d$). The micelle may adjust its size and shape so as to achieve optimal packing of the amphiphiles. We assume the hydrophobic interior to be compact and the hydrocarbon−water interface to be smooth everywhere. The vector **b** marks one specific chain director, pointing from the hydrocarbon−water interface to the mid-axis.

2.2 Micellar Energy and Shape. Consider an elongated, rodlike micelle composed of N amphiphiles. Figure 1 illustrates our "initial" structural model of such a micelle, which consists of a cylindrically symmetric middle part, smoothly joined by two globular, approximately spherical, endcaps.

We refer to this model as "initial" because the final, optimal shape of the micelle will be determined by minimizing its internal free energy, $\mu^0(N)$, subject to (some simple) structural and packing constraints. Throughout the discussion, we shall assume that the hydrocarbon−water interface is smooth and well defined, and that the hydrophobic core is incompressible, i.e., $V = N\nu$

With every point on the hydrocarbon−water interface, we can associate a vector, the *chain director*, **b**, whose origin is at the interface and whose direction coincides with the (conformationally averaged) end-to-end vector of a chain originating at this point. (The headgroups reside just outside the interface.) By symmetry, all chain directors point toward the main micellar axis. We define the length of the director, $b = |\mathbf{b}|$, as the distance between the chain origin and the mid-axis. We may refer to b as the effective local "chain extension", yet it should be noted that b is not the average end-to-end length of the chain. (The average chain length in both spherical and cylindrical micelles is smaller than their respective radii, b.) We make the additional assumption that the local director is always oriented normal to the corresponding surface area element. (The validity of this assumption is discussed below.)

From the last assumption, it follows that the micelle must consist of a central region where the chain directors point toward (different points on) the main micellar axis, and two endcaps, within which all chain directors are pointing toward one point (also located on the main axis). Because the directors are normal to the interface the endcaps are, necessarily, spherical (devoid of the section defined by the angle $\pi/2 - \theta_0$, Figure 1). Their size and shape, as dictated by their radius $b = b_s$, are variational parameters, to be determined by minimizing $\mu^0(N)$. Within the cylindrical middle part b is not a constant, but rather, a continuous function of the position of the director's tip on the main axis. The b profile in this region is also dictated by the minimum of $\mu^0(N)$.

The internal energy of the micelle can now be expressed as a sum of contributions from the endcaps (μ_s^0) and the cylindri-

cal middle part (μ_c^0)

$$\mu^0 = \mu_s^0 + \mu_c^0 = \int_{sph} dN\, f + \int_{cyl} dN\, f \qquad (11)$$

where the integrations extend over all amphiphiles constituting the spherical and cylindrical parts, respectively. In minimizing $\mu_0(N)$, we shall allow variations in the size and shape of these regions, subject to the requirement that they smoothly join each other, and that $N_s + N_c = N$, (equivalently, $V_c + V_s = V$). Here, $N_c = \int_{cyl} dN = V_c/\nu$ and $N_s = \int_{sph} dN = V_s/\nu$ are the numbers of molecules in the cylindrical body and the spherical endcaps ($N_s/2$ in each endcap). In our search for the minimum of $\mu^0(N)$, we shall assume that the micelle is symmetric with respect to rotation around its long axis and with respect to reflection through the plane normally intersecting this axis between the two endcaps.

In general, the packing free energy of amphiphiles in micellar aggregates depends not only on the average area per headgroup at the interface (a) and the local chain extension (b) but also on the "tilt angle" specifying the orientation of the chain director with respect to the hydrocarbon−water interface (or, alternatively, with respect to the main axis). In principle, an elastic, chain tilting contribution[20,21] may be extracted from, or explicitly added to, our expression for f (see eqs 8, 9, and 10). The tilt angle would then be an independent degree of freedom, and a corresponding tilt modulus κ_t would determine the stiffness of the hydrocarbon tails with respect to changes in the tilt angle. Preliminary calculations (which are not reported here) reveal that the inclusion of the tilt degree of freedom greatly complicates the model, without significantly affecting its predictions. Furthermore, no reliable experimental or theoretical information is available so far regarding the magnitude of κ_t. Consequently, in all the calculations presented below, we shall assume that all of the chain directors are oriented normally to the hydrocarbon−water interface, as they do, for instance, in perfectly symmetric spherical and cylindrical micelles, as well as in all (fluid) lipid bilayers. It may be noted that this assumption is commonplace[22] in the theory of lipid layer perturbations, showing generally good agreement with experiment.[23−25]

From the assumptions that the local chain director is normal to the interface and that the hydrophobic core is incompressible, it follows that the local chain extension b uniquely determines the local area per headgroup a, (see next section). Consequently, the local free energy f becomes a function of the local director b, and the minimization of $\mu_0(N)$ involves a simultaneous variation of b, for all chains constituting the micelle. Because $\mu^0(N) = \mu_c^0 + \mu_s^0$, it is instructive to first consider, separately, each of the two contributions to $\mu^0(N)$, and then describe their coupling in an integrated micelle.

Cylindrical Body. Figure 2 illustrates schematically the "left" half of the cylindrical body of the micelle; the right half is its mirror image. Using $x = 0...2d$ to denote the position of the director tip along the micellar main axis this half corresponds to the region $0 \le x \le d$. We shall use $b(x)$ to denote the director length ending at x, and $\pi/2 - \theta$ for the angle between the director and the main axis. Thus $h(\bar{x}) = b \cos\theta$ is the "height" of the hydrophobic core (i.e., the normal distance from the axis to the interface) at the point $\bar{x} = x + b \sin\theta$. At $x = d$, which marks the position of the reflection symmetry plane, the director **b** is normal to the x-axis, hence $\theta = 0$ and $h = b$. At the border with the spherical endcap, $x = 0$, $\theta = \theta_0$ and $b = b_s$. Because the director is normal to the interface, it follows that $\sin\theta = -b'$, implying $h(x - bb') = b\sqrt{1-b'^2}$, with $b' = db/dx$ (see Figure 2).

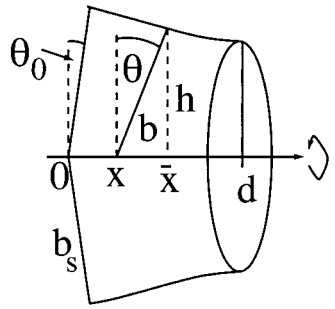

Figure 2. Schematic illustration of the ("left half") of the cylindrical middle part. Its shape is fully specified by the director profile $b(x)$. The chain director is everywhere normal to the hydrocarbon−water interface. The thickness of the hydrophobic core at $\bar{x} = x - bb'$ is thus given by $h(\bar{x}) = b\sqrt{1-b'^2}$.

The total volume, V_c, and surface area, A_c, of the cylindrical body can be expressed in the form $V_c = \int_{cyl} dN/\nu = 2\int_0^d dx\, g_V$ and $A_c = 2\int_0^d dx\, g_A$, with

$$g_V = 2\pi b^2\left[\frac{1}{2}(1 - b'^2) - \frac{1}{3}bb''\right]$$

$$g_A = 2\pi b[1 - b'^2 - bb''] \qquad (12)$$

These functions express, respectively, the local (circular) volume and area elements, corresponding to all chains whose directors end between x and $x + dx$. Equivalently, $dN = (g_V/\nu)dx$ is the number of chain directors ending at x,$x + dx$, and $dA = g_A dx$ is the area element from which these directors emanate. Thus, $a = dA/dN = \nu g_A/g_V$ is the local area per molecule at the hydrocarbon−water interface. Both g_V and g_A depend only on $b(x)$. The explicit expressions in eqs 12 are derived using the requirement that the local director is normal everywhere, with respect to the interface. For any given function $b(x)$, the overall number of chains in the cylindrical part is $N_c = V_c/\nu$.

The contribution to $\mu^0(N)$ arising from the cylindrical region, see eq 11, is now given by

$$\mu_c^0 = 2\int_0^d dx \frac{g_V}{\nu} f = 2\int_0^d dx\, \bar{f} \qquad (13)$$

with $\bar{f} \equiv g_V f/\nu$ denoting the (one-dimensional) free energy density of the cylindrical body along its rotational axis.

Recall that unidimensional micellar growth will only take place if the optimal packing geometry of the amphiphiles is cylindrical. Namely, once the micelles get very long most amphiphiles will pack in the central regions of their cylindrical bodies, where $b = b_e$ is the optimal packing radius; $1 > b_e/l > 2/3$ (corresponding to $3 > p > 2$ for the packing parameter). We shall focus here on systems with $p = y$, so that $b_e = b_o = b^*(cyl) = 2\nu/a_o$ optimizes both headgroup and chain packing. In very long micelles ($d \gg b$), most molecules will pack with $b = b_o$ where $f = f_{cyl} = 0$.

Introducing $s = b/b_o - 1$ as a measure of the local chain stretching, relative to its unperturbed length b_o, we can express $\bar{f}$ as a power series in s and its derivatives s' and s''. Keeping terms up to second order in these variables one finds

$$\frac{\bar{f}}{2\gamma\pi b_o} = \left(\frac{b_o^2}{3}s'' + s\right)^2 + \tilde{\tau}s^2 \qquad (14)$$

with $\tilde{\tau} = b_o^3\tau/(2\gamma\nu)$ denoting the dimensionless chain stretching modulus.

Substituting $\bar{f}$ into eq 13, we are seeking the function $s(x)$ which minimizes μ_c^0. This, stationary, $s(x)$ profile must thus fulfill the Euler−Lagrange equation

$$\frac{b_o^4}{3}s'''' + 3(1+\tilde{\tau})s + 2b_o^2 s'' = 0 \qquad (15)$$

Because $\tilde{\tau} > 0$ the general solution is of the form $s(x) = \sum_{i=1}^{4} c_i s_i(x)$, where the c_i's are constants and the four functions $s_i(x)$ are

$$s_1(x) = \exp(-x/\xi_1)\cos(x/\xi_2)$$
$$s_2(x) = \exp(-x/\xi_1)\sin(x/\xi_2)$$
$$s_3(x) = \exp(x/\xi_1)\cos(-x/\xi_2)$$
$$s_4(x) = \exp(x/\xi_1)\sin(-x/\xi_2) \qquad (16)$$

The two characteristic lengths, ξ_1,ξ_2 are

$$\xi_1 = \frac{b_o\sqrt{2/3}}{\sqrt{\sqrt{1+\tilde{\tau}}-1}},\ \xi_2 = \frac{b_o\sqrt{2/3}}{\sqrt{\sqrt{1+\tilde{\tau}}+1}} \qquad (17)$$

The c_i's are dictated by the boundary conditions of the problem, namely

$$s(0) = s_0,\ s'(0) = -\frac{\theta_0}{b_o},\ s'(d) = 0,\ s'''(d) = 0 \qquad (18)$$

The first two conditions correspond to the border between the cylindrical body and the spherical endcap, ensuring that the chain length at $x = 0$ and the shape of the hydrophobic region of the cylindrical body match the corresponding characteristics of the spherical cap exactly. Both s_0 and θ_0 are still undetermined. The last two boundary conditions express the mirror symmetry of the micellar shape at $x = d$. They follow from the smoothness of the hydrocarbon−water interface and from the relation $b(d - x) = b(d + x)$. Note that because we have used the expanded rather than the full form of $\bar{f}$, our result for μ_c^0 will be valid up to quadratic order in s_0 and θ_0.

Calculation of the c_i's in the general case leads to lengthy expressions that we avoid reporting here. These expressions are considerably simpler, but still quite cumbersome in the "long micelle limit", $d \to \infty$, i.e., when the endcaps are far apart from each other. In this limit the result is

$$c_1 = s_0,\ c_3 = c_4 = 0$$
$$c_2 = \frac{s_0\sqrt{-1+\sqrt{1+\tilde{\tau}}} - \theta_0\sqrt{2/3}}{1+\sqrt{1+\tilde{\tau}}} \qquad (19)$$

Using eqs 13, 14, 16, and 19 one finds that $\mu_{c,\infty}^0 = \mu_c^0(d \to \infty)$ is given by

$$\frac{\mu_{c,\infty}^0}{2\gamma\pi b_o^2} = -\frac{4}{3}\frac{\tilde{\tau}s_0\theta_0}{1+\sqrt{1+\tilde{\tau}}} + 2\sqrt{\frac{2}{3}}\sqrt{-1+\sqrt{1+\tilde{\tau}}}\left(s_0^2\sqrt{1+\tilde{\tau}} + \frac{1}{3}\theta_0^2\right) \qquad (20)$$

We conclude this section with a brief discussion of the limit $\tau = 0$, in which case the chain stretching energy does not contribute to the molecular packing free energy, and $f = f_o$ is fully represented by the OFM. In this limit, the energy of the micelle is dictated solely by the local deviations of the molecular cross-sectional area, a, from its equilibrium value a_o. From eq 17, we see that one of the characteristic lengths, namely ξ_1, diverges, whereas $\xi_2 = \xi_2(\tilde{\tau} = 0) = b_o/\sqrt{3}$ remains finite. This implies that no decay length can be associated with the perturbation of the micellar profile, $s(x)$, which oscillates periodically according to ξ_2. Indeed, for $\tilde{\tau} = 0$, we see from eq 14 that any micellar perturbation fulfilling the equation $s + b_o^2 s''/3 = 0$ implies $\mu_c^0 = 0$, indicating that optimal packing, i.e., $a = a_o$, can be satisfied even though the micellar body is an "oscillatory" rather than a straight cylinder. More generally, it is possible to show that (in the limit $d \to \infty$) for any given perturbation of the cylindrical body at $x = 0$ (as expressed through s_0 and θ_0) there is a nondecaying sinusoidal perturbation profile that ensures $a \equiv a_o$ everywhere, implying $\mu_c^0(\tau = 0, d \to \infty) \equiv 0$, in agreement with eq 20 for $\tau = 0$. We thus arrive at the conclusion that a nonvanishing $\tau > 0$ ensures an exponential decay of any local micellar perturbation, like the one induced by the presence of a spherical endcap. Without the chain packing contribution to the molecular free energy ($\tau = 0$) the (sufficiently long) micelle can adopt a sinusoidal perturbation profile at no energy cost.

Spherical Endcaps. Following our assumption that the chain directors are perpendicular to the hydrocarbon−water interface, the endcaps are necessarily spherical, devoid of the conical section defined by the contact angle with the cylindrical middle part θ_0. Both θ_0 and the sphere radius b_s are allowed to adjust so as to minimize the total free energy of the micelle.

The number of amphiphiles in the two endcaps is

$$N_s = \frac{4\pi b_s^3}{3\nu}(1+\sin\theta_0) \approx \frac{4\pi b_s^3}{3\nu}(1+\theta_0) \qquad (21)$$

where the second equality corresponds to the case of small (second order in θ) perturbations, in which level we have also treated the cylindrical middle part. The contribution of the two endcaps to $\mu^0(N)$ is

$$\mu_s^0 = N_s\left[\gamma a_s\left(1-\frac{a_o}{a_s}\right)^2 + \tau(b_s - l)^2\right] \qquad (22)$$

with $a_s = 3\nu/b_s$, as appropriate for spherical micelles. The height matching condition at the border between the endcaps and the cylindrical body implies $s_0 = b_s/b_o - 1$.

In our discussion above of the cylindrical middle part, we have derived an expression for μ_c^0 by minimizing the interfacial (or $b(x)$) profile of this section of the micelle, for given values of the structural parameters d, b_s and θ_0. This μ_c^0 can be added to $\mu_s^0 = \mu_s^0(b_s,\theta_0)$ to obtain the free energy of a micelle, $\mu^0 = \mu_c^0 + \mu_s^0$, for the given d, b_s, and θ_0. Further minimization of μ^0 with respect to θ_0 and b_s, yields $\mu^0(d)$ − the internal free energy of a micelle of *length* d. Because the shape, and hence the volume V, of this micelle are known its aggregation number is given by $N = V/v$. This has been the procedure employed in our calculations to evaluate the $\mu^0(N)$'s. It should be noted, however, that this procedure actually yields an upper bound for $\mu^0(N)$ because we have optimized N for the given d, rather than d for the given N. For large d, the upper bound coincides with the exact value because N varies linearly with d. Thus, the shape and energy of the endcaps of long micelles, as well as the

average micellar size of such micelles are calculated accurately. Deviations, if any, may only appear for intermediate N values. As we shall see, however, if a second CMC shows up with the approximate μ^0 it will be even more pronounced with the exact (possibly slightly lower) values.

Results and Discussion

In this section, we present numerical results for $\mu^0(N)$ and size distributions $\{X(N)\}$ for micelles composed of P—$(CH_2)_{13}$—CH_3 amphiphiles, with P symbolizing the (unspecified) polar headgroup of these molecules. The volume and length of the C-14 tails are given by $v = 405$ Å^3 and $l = 17.8$ Å, respectively. For the effective hydrocarbon−water surface tension, we use $\gamma = 0.12\ k_BT/$Å^2. The packing characteristics of such amphiphiles in different micellar environments have previously been studied[19] based on a detailed, molecular-level, model for the chain packing free energy, f_t. (The headgroup contribution has been modeled there using the same OFM scheme described in Sec. 2.1.) Our phenomenological expression, $f_t = \tau(b - b^*)^2$ (eq 10), shows good agreement with the numerical results obtained using the molecular-level calculations of f_t. More explicitly, for C-14 chains, these calculations suggest $\tau \approx 0.02 k_BT/$Å^2 for both cylindrical and spherical micelles. The values of b^* are different: $b^*(\text{sph}) = l$, whereas (to a good approximation) $b^*(\text{cyl}) \approx 0.8l = 14.2$ Å. The above values of τ and the b^*'s will be used in all the calculations reported below.

We note again that for $b^*(\text{cyl}) = b_o = b_e$, the cylindrical geometry offers optimal packing for both the headgroups and the hydrophobic tails. Furthermore, $b^*(\text{cyl}) = b_o = 0.8l$ implies $p = y = 2l/b_o = 2.5$ for the packing parameter, i.e., well within the range $(2 < p < 3)$ where cylindrical micelles are more favorable than any other aggregation geometry, particularly spherical micelles (which prevail when $y \geq 3$). All the results presented below are derived for $y = p = 2.5$. For this choice of y, one finds $f^{\text{cyl}}(b = b_o) = 0$ and $f^{\text{sph}}(b_s \approx l) = \gamma a_o(3/y)(1 - y/3)^2 \approx 0.23$, for the (minimal) free energy per molecule in cylindrical and spherical geometries, respectively. Similar micellar shapes and size distributions are expected for all amphiphiles which strongly prefer the cylindrical packing geometry.

Micellar Energy and Shape. Because of the prohibitive energy penalty inflicted by the creation of a void in its hydrophobic core, the maximal radius of the minimal, spherical $(N = M)$, micelle cannot exceed $b_s = l$, even though our choice of $y < 3$ would favor a larger value for b_s. Contraction of the micelle to $b_s < l$ is also highly unfavorable because it involves an increase in both f_o and f_t, see eq 22. This leads to a very steep minimum of $\mu_s^0(b_s)$ at $b_s = l$, implying that a substantial force would be necessary to either expand $(b_s > l)$ or compress $(b_s < l)$ the micelle. A compression force is actually exerted on the spherical endcaps of somewhat larger micelles $(N > M)$ owing to the tendency of the cylindrical middle part to adopt its optimal radius $b_o < l$. Our numerical calculations reveal, however, that for all $N > M$ this force is not strong enough to cause a noticeable contraction of the endcaps. Thus, their radius is maximal, $b_s = l$, irrespective of N. Consequently, their shape is fully specified by the contact angle θ_0.

The minimal aggregation number, corresponding to a perfectly spherical micelle, is $M = N_s(b_s = l, \theta_0 = 0) = 4\pi l^3/(3v) = 58$. Two other important structural characteristics, whose values are dictated by our initial choice of molecular parameters are the characteristic lengths ξ_1 and ξ_2; (see eq 17). For $b_o = 14.2$ Å and $\tau = 0.02 k_BT/$Å^2 we get $\xi_1 = 22.7$ Å and $\xi_2 = 7.7$ Å. Note that the decay length of the (thickness) perturbation of the cylindrical body, ξ_1, is comparable to the micelle diameter.

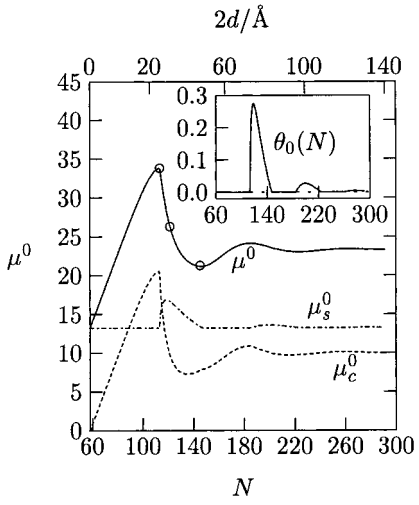

Figure 3. Packing free energy of a linear micelle, $\mu^0(N) = \mu_c^0(N) + \mu_s^0(N)$, and its two components (in k_BT's) as a function of the aggregation number N, for micelles composed of C-14 amphiphiles, (with $\tau = 0.02\ k_BT/$Å^2 and $y = 2.5$). The endcap radius is $b_s = l$ for all N. The inset shows the variation in the contact angle $\theta_0(N)$. The circles mark selected aggregation numbers corresponding to micelles whose shapes are shown below, in Figure 5.

Figure 3 shows how $\mu^0(N)$, as well as its two components $\mu_s^0(N)$ and $\mu_c^0(N)$ vary with the micelle size N. The inset shows how the corresponding variation in the contact angle, $\theta_0(N)$.

The energy of the minimal micelle $(N = M)$ can be obtained from eq 22 for $N_s = M$. Using $b_s = l$, $a_s = 3v/b_s$, $a_o = yv/l$ we find $\mu^0(M) = \mu_s^0(\theta_0 = 0) = 3M\gamma v(1 - y/3)^2/l$, yielding $\mu^0(M) = 13.2$ for $y = 2.5$; equivalently $f^{\text{sph}} = \mu^0(M)/M = 0.23$. (Recall that all energies are expressed in units of k_BT.) A cylindrical middle part begins to form as soon as N exceeds M. Initially, i.e., for $d \ll \xi_1$, the middle part is still a straight cylinder of length $2d$ and radius $b_c \approx b_s = l$, implying $N_c \approx 2d\pi l^2/v$. Using eqs 13 and 14 with $s(x) \equiv s_0 = y/2 - 1$ we obtain

$$\frac{d\mu_c^0}{dN} \approx \frac{4\gamma v}{ly}\left(1 - \frac{y}{2}\right)^2(1 + \tilde{\tau}) \approx 0.45 \qquad (23)$$

in agreement with the results in Figure 3. The linear behavior $\mu_c^0 \approx N$ continues until the micelle nearly doubles its size ($N \approx 110$). Throughout this region, $\theta_0 = 0$ and hence both $N_s = M$ and μ_s^0 are constant, with μ_c^0 providing an increasingly larger contribution to $\mu^0(N)$. At $N \approx 110$, the major part of the excess free energy of the micelle is concentrated in the cylindrical middle part, which is a result of its highly unfavorable chain packing in the vicinity of the endcaps.

Eventually, when $N - M$ becomes sufficiently large (in our example at $N \approx 2M$), the energetic price of adding molecules to a cylindrical body of (nonoptimal) radius $b_c = b_s$ becomes intolerable, at least in comparison to another packing option. Namely, to narrow cylindrical body toward its optimal radius b_o $(b_o < b_s)$. To enable a gradual narrowing of the cylinder's radius, the micelle must first increase the contact angle θ_0, implying a certain increase in the endcap energy that partly compensates (but cannot compete with) the gain in packing the molecules in the cylindrical body.

This change in the growth mode of the micelle is responsible for the appearance of the pronounced maximum in $\mu^0(N)$. Following this maximum, one observes a damped oscillatory behavior of $\mu^0(N)$. The period and decay length of these oscillations is dictated by the two characteristic length scales, ξ_1 and ξ_2. Similar, oscillating perturbation energy profiles have

been predicted for lipid membranes containing hydrophobic inclusions (such as integral proteins) whose height does not match the equilibrium thickness of the host lipid membrane.[22] The present analogue of these inclusions are the spherical endcaps of the micelle. However, in contrast to rigid inclusions in membranes, the endcaps can adjust their size (i.e., θ_0) so as to lower the total free energy of the aggregate.

It should be mentioned that although the maximum in $\mu^0(N)$ is very real and relevant for a realistic range of molecular packing parameters, the following oscillations are intimately associated with one of the simplifying assumptions of our model; namely, our neglect of the tilt degree of freedom, as reflected by our assumption that the chain director is everywhere perpendicular to the hydrocarbon−water interface. This conclusion is corroborated by preliminary calculations (not reported here) in which the tilt degree of freedom is taken into account, as well as by detailed calculations on hydrophobic inclusions in membranes. In both cases, allowing the amphiphile chains to optimize their tilt angle largely reduces the oscillations and results in essentially smooth energy and interfacial profiles.[21,26] Thus, we shall not attribute special physical significance to the oscillatory region of $\mu^0(N)$.

The final shape and energy of the endcaps are established when d significantly exceeds the perturbation length ξ_1. In this (formally $N \rightarrow \infty$) limit we find $\theta_0 \approx 0$. We can thus calculate μ_c^0 from eq 20 with $s_0 = y/2 - 1$ and $\theta_0 = 0$. For our molecular parameters this yields $\mu_c^0 = 10.0$, in agreement with Figure 3.

Recall that the simple spherocylinder model predicts that the excess endcap energy $\mu^0(N) - N f^{cyl} = 2\delta$ (see eq 1) is the same for all $N \geq M$. By contrast, from Figure 3, it is apparent that the asymptotic endcap energy, $2\delta = \mu^0(N \rightarrow \infty)$, is considerably larger than the excess energy of the minimal, spherical, micelle $\mu^0(M)/2$. Namely, $\delta = 11.6$ as compared to $\mu^0(M)/2 = 6.6$. This means, as we have already noted, that as soon as the spherical micelle begins to elongate its internal energy must increase considerably (the difference between 2δ and $\mu^0(M)$ is $10k_BT$) before the final endcap energy reaches its final value. This internal energy barrier, which corresponds to the micellar size region where the endcaps still "interact" with each other, is a necessary condition for the appearance of a second CMC in the micellar growth process (see below). More precisely, recall that micellar growth is driven by the fact that the packing free energy *per molecule*, $\mu^0(N)/N$, is a decreasing function of N. The absence (or very small population) of certain intermediate-size micelles requires that their corresponding $\mu^0(N)/N$ will be larger than those of both smaller and larger micelles, i.e., a maximum should appear in the function $\mu^0(N)/N$, as was first pointed out by Porte et al.[11] For our specific system, this function is shown in Figure 4, revealing a significant maximum at $N \approx 100$.

The evolution of the packing geometry in the early stages of micellar growth is illustrated for three values of N ($N = 113$, 121, 146) in Figure 5. Among these three examples the largest packing energy, μ^0, corresponds to the smallest ($N = 113$) micelle, reflecting the highly unfavorable packing of amphiphiles in its frustrated cylindrical middle part. The amphiphile chains in this region of the micelle are highly stretched in comparison to their optimal length, and their headgroups are densely crowded. For $N = 121$, we observe a substantial decrease in the thickness of the micelle around $x = d$, resulting in a pronounced bulging of the micellar ends. This effect is amplified by an increase in size of the spherical endcap. In fact, for $N = 121$ the size of the endcaps, as expressed through θ_0, is maximal. For larger N, the endcaps begin separating from each other and,

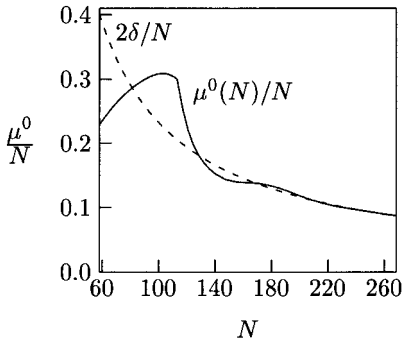

Figure 4. Average packing free energy per molecule in a micelle, $\mu^0(N)/N$, as a function of the aggregation number N. The dashed curve, showing $2\delta/N$, corresponds to spherocylindrical micelles with the same asymptotic endcap energy.

concomitantly, the contact angle $\theta_0 \rightarrow 0$. At $N = 146$, the internal energy of the micelle shows a local minimum, as seen in Figure 3.

When N gets very large, corresponding to $d \gg \xi_1$, the endcaps no longer interact with each other, and their final shape is well established. This shape is illustrated in Figure 6, indicating that the endcaps are bulkier than the cylindrical body.

3.2 Micellar Growth. Substituting the calculated values of $\mu^0(N)$ (Figure 3) into eq 6, we obtain the micellar size distribution, $\{X(N)\}$, as shown in Figure 7 for several different values of the total mole fraction of (micellized) amphiphiles in solution, X.

The most pronounced feature of these size distributions, apparent for all X, is the "gap" around $N \approx 100$, which clearly divides $\{X(N)\}$ into two micellar populations. One of these populations involves only small (and hence globular) micelles whose aggregation numbers are not much larger than that of the minimal size, $M \approx 60$ in the present case. The other population involves all larger micelles. The nonmonotonic behavior of $X(N)$ is markedly different from the predictions of the spherocylinder model, where $X(N)$ is a smoothly varying function of N, showing a single wide maximum that gradually increases with X. (According to the spherocylinder model $X(N)$ is maximal at $N = \langle N \rangle/2 = \sqrt{X}\exp(\delta)$.)

As noted already in Sec. 1, a gap in the size distribution signifies a second CMC behavior. Namely, when X is low, all of the micelles are small, as demonstrated for instance by curves (*a*)−(*c*) in Figure 7. (Note that the logarithmic scale greatly amplifies the population of larger micelles; their overall concentration is negligibly small for all $X \leq 0.3 \times 10^{-4}$, see below. Note also the concentration of micelles of size N is proportional to $X(N)/N$.) The overall mole fraction of amphiphiles aggregated in small micelles continues to increase with X, reaching a saturation value at some well-defined overall concentration $X = X_{2c}$ ($X_{2c} \approx 0.3 \times 10^{-4}$ in our model system); X_{2c} is the second CMC. The long micelle population begins to increase as soon as X exceeds X_{2c}. In this regime, as clearly seen in Figure 7, the average aggregation number increases continuously with X. Actually, for $X \gg X_{2c}$ the average size of the long micelles obeys the familiar growth law $\langle N \rangle \approx 2\sqrt{X}\exp(\delta)$, see eq 2. The size distribution shown in Figure 7 are very similar to those observed experimentally by Kato et al.[13] for $C_{12}E_5$ surfactants.

At this point, we reiterate that our calculations are relevant for linear micelles in the dilute solution limit. Thus, they do not account for intermicellar interactions or for "higher order" structural effects such as micellar flexibility or branching. Note,

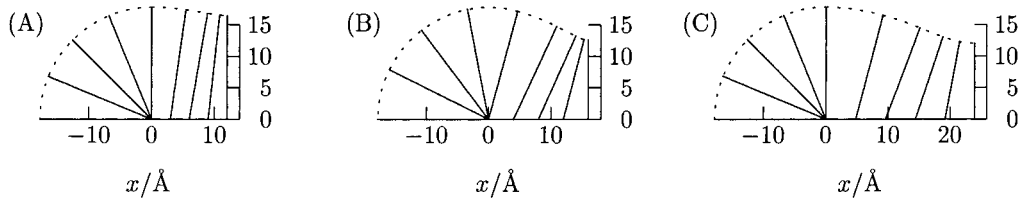

Figure 5. Micellar structures for $N = 113$ (A), $N = 121$ (B), and $N = 146$ (C). The dashed line marks the hydrocarbon−water interface. Chain directors are shown at arbitrary positions.

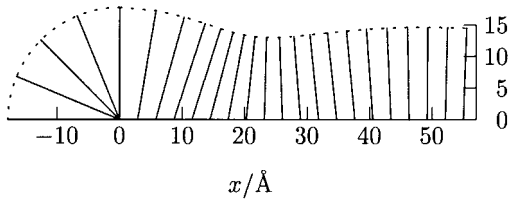

Figure 6. Final structure of the endcap region, as calculated for very long micelles. These micelles grow by adding molecules to the central region of the cylindrical body, where amphiphile packing is optimal. Chain directors are shown at arbitrary positions.

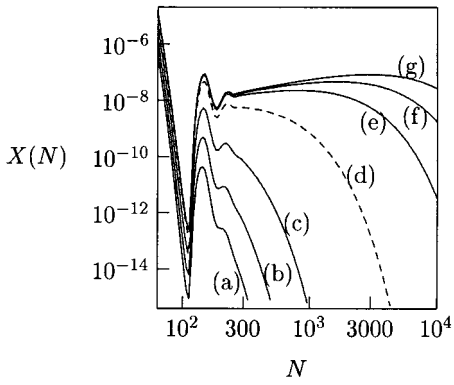

Figure 7. Micelle size distributions, $X(N)$, for different total amphiphile concentrations X. $X = 0.01 \times 10^{-4}$, (a); 0.03×10^{-4}, (b); 0.09×10^{-4}, (c); 0.27×10^{-4}, (d); 0.81×10^{-4}, (e); 2.43×10^{-4}, (f); and 7.29×10^{-4}, (g). The value of X corresponding to the dashed curve (d) is close to the second CMC.

however, that neither intermicellar interactions nor flexibiity or branching are very relevant for the endcap structure or the self-assembly behavior around the second CMC.

One marginal feature of the size distributions shown in Figure 7 involves the additional peak at $N \approx 150$ and the minor, damped, oscillations at $N \sim 180-250$. This behavior is a consequence of the local minimum and weak oscillations of $\mu^0(N)$ in this regime, as seen in Figures 3 and 4. As explained in the previous section, one should not attribute a special physical significance to these oscillations, whose origin is a simplifying assumption of our structural model. From Figure 7, it is apparent that the overall concentration of these "medium-size" micelles, ($N \approx 150-250$), is always small with respect to either the small ($N \geq M \approx 60$) or large ($N \gtrsim 250$) micelle populations. Furthermore, their concentration saturates at just a slightly larger value than the saturation concentration of the very small micelles. Thus, to simplify the forthcoming discussion of the second CMC, we shall regard the "medium-size" micelles as belonging to the small micelle population. For our model system this means that the long-micelle population correspond to $N \geq L \approx 250$.

The second CMC behavior is quantitatively demonstrated in Figure 8 which shows how the overall populations of small (X_s) and large (X_l) micelles vary with the total amphiphile concentration, X.

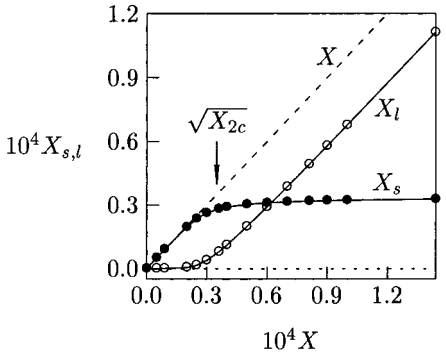

Figure 8. Change in amphiphile populations incorporated in small (X_s) and long (X_l) micelles with the total concentration, X. Small micelles correspond to aggregation numbers $M \leq N \leq L = 250$. The dashed line shows $X = X_s + X_l$. The arrow marks the value of the second CMC, X_{2c}, as predicted by eq 34 (see below).

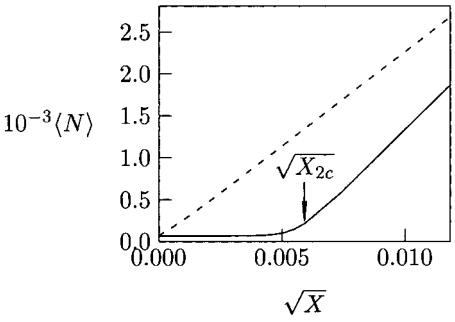

Figure 9. Weight average size $\langle N \rangle$ as a function of $\sqrt{X}$. The limiting behavior for large X is given by the spherocylinder model (dashed line), namely $\langle N \rangle = 2 \exp(\delta)\sqrt{X}$, with $\delta = \mu^0(N \rightarrow \infty)/2$ denoting the asymptotic value of the endcap energy. The numerical value $\delta = 11.6$ is dictated by the results shown in Figure 3. The arrow marks the value of the second CMC, X_{2c}, as predicted by eq 34.

These two populations are defined by

$$X_s = \int_M^L X(N)\, dN,\ X_l = \int_L^\infty X(N)\, dN \qquad (24)$$

with $L = 250$. The evolution of X_s and X_l as a function of X exhibits very different behaviors in the pre- and post-second CMC regimes. Below the second CMC, or more precisely for $X \leq X_{2c} - \Delta$ ($\Delta > 0$), we find $X = X_s$; $X_l \approx 0$, whereas for $X > X_{2c} + \Delta$ the small micelle concentration is essential constant, $X_s \approx X_{2c}$, whereas the long micelle population $X_l = X - X_{2c}$ increases linearly with X. The concentration interval Δ measures the "sharpness" of the second CMC. For our model system, $X_{2c} \approx 0.3 \times 10^{-4}$ and $\Delta \approx 0.1 \times 10^{-4}$.

Finally, in Figure 9, we show how the weight average aggregation number

$$\langle N \rangle = \int_M^\infty NX(N)dN \Big/ \int_M^\infty X(N)dN \qquad (25)$$

increases with the total concentration.

Below the second CMC, all amphiphiles are self-assembled in small micelles, implying $\langle N\rangle \approx M$. As soon as X exceeds X_{2c} (the arrow in Figure 9 marks the prediction for X_{2c} according to eq 34, see below), all added amphiphiles are incorporated into long micelles whose size distribution is governed by the same principles dictating the growth of spherocylindrical micelles. In particular, for $\langle N\rangle \gg L$ their average size increases with X according to the usual growth law $\langle N\rangle = 2\sqrt{X}\exp(\delta)$ (see eq 2), with $\delta = \mu^0(N \to \infty)/2 = 11.6$, as found in Figure 3. For comparison, we also show how $\langle N\rangle$ increases for spherocylindrical micelles with the same endcap energy δ.

3.3 Second CMC. Equipped with the numerical examples from the previous sections, we conclude the discussion with a general theoretical analysis of the molecular and thermodynamic characteristics of the second CMC.

We have defined a long micelle ($N \geq L$) as one whose cylindrical body is long enough to ensure that its two endcaps do not interact with each other. In other words, the endcaps have already adopted their asymptotic structure. Regardless of the endcap structure, the internal energy of these micelles is given by $\mu^0(N) = N f^{cyl} + 2\delta$, where f^{cyl} is the free energy per molecule in the (optimally packed) cylindrical body and δ is the asymptotic endcap energy. Without loss of generality, we can set $f^{cyl} = 0$, as we also did in our calculations. Thus, for $N \geq L$ we have $\mu^0(N) = 2\delta$, with L denoting the aggregation number of the smallest long micelle. In the simple spherocylinder model $L = M$, and $\mu^0(N) = 2\delta$ applies to all micellar sizes.

As we have seen in the previous sections, the asymptotic form of $\mu^0(N)$ is not applicable for small micelles ($M \leq N \leq L$), whose endcaps are still interacting with each other. Introducing the function $g(N)$ to account for the deviations of $\mu^0(N)$ from its asymptotic value we write

$$\mu^0(N) = 2\delta - g(N) \tag{26}$$

where $g(N) \equiv 0$ for all $N \geq L$. Referring to Figure 3, we note that $g(N) \neq 0$ in the small micelle regime, $58 \leq N \leq 250$. Note in particular that $g(N)$ is positive for the very small micelles where $N \approx M$. Most significantly, $g(N \approx M) \approx 10$ (in k_BT's), implying $\exp[g(N \approx M)] \gg 1$.

Substituting eq 26 into eq 6 we obtain

$$X(N) = N\exp(-2\delta)\exp[g(N) + N\mu] \tag{27}$$

where it should be noted that (since $g(N \geq L) = 0$) the chemical potential must be negative ($\mu < 0$), to ensure convergence of $X = X_s + X_l$.

For the total mole fraction of amphiphiles in long micelles ($g(N) = 0$), we find

$$X_l = \frac{\exp(-2\delta)}{\mu^2} \tag{28}$$

which holds for $L|\mu| \ll 1$. Note that this condition is equivalent to the requirement $X_l \gg \exp(-2\delta)$. For systems exhibiting the formation of long micelles (at large enough X), the endcap energies are typically several tens of k_BT's; e.g., in our model system, $2\delta \approx 25$. Thus, this condition is already satisfied for extremely small values of X_l; e.g., for $X_l \approx 1.1X_{2c}$ or even less, as will be verified below. Because, for (most of) the small micelles $g(N) \approx 1...10$, it follows that as soon as X_l starts approaching X_{2c}, we can safely set $N|\mu| \ll g(N)$ for (most) $M \leq N \leq L$. Thus, close to X_{2c}

$$X_s = \exp(-2\delta)\int_M^L dN\, N\exp[g(N) + N\mu] \approx \exp(-2\delta)\int_M^L dN\, N\exp[g(N)] \equiv X_s^{(1)} \tag{29}$$

where $X_s^{(1)}$ is the first moment, $m = 1$, of the function $\exp[-2\delta + g(N)]$, whose m'th moment is defined by

$$X_s^{(m)} = \exp(-2\delta)\int_M^L dN\, N^m\exp[g(N)] \tag{30}$$

Because $X_s \approx X_s^{(1)} =$ constant is the saturation value of the small micelle concentration, it may well be identified as the value of the second CMC, X_{2c}. Yet, to complete the identification of $X = X_{2c} = X_s^{(1)}$ as the second CMC, we still need to verify that the transition is sharp. That is, we have to show that over a narrow concentration range, in the vicinity of X_{2c}, the rate of change of the small micelle concentration changes rapidly from $dX_s/dX \approx 1$ to $dX_s/dX \approx 0$. In other words, at X_{2c} the second derivative, d^2X_s/dX^2, should be large and negative. Equivalently, the requirement for a well-defined second CMC can be formulated as follows. Let X' ($X' \approx X_{2c}$) denote a specific concentration in the vicinity of the CMC, such that

$$\left(\frac{dX_s}{dX}\right)_{X'} = \frac{1}{k} \tag{31}$$

where $k > 1$ is some finite positive (not necessarily integer) number. The second CMC is well-defined if a small increase in X' implies a large increase in k.

An operational definition of the second CMC can be obtained[27] by choosing some (arbitrary) $k > 1$ and requiring $(dX_s/dX)_{X_{2c}} = 1/k$. From eq 29

$$\left(\frac{dX_s}{dX}\right) = \exp(-2\delta)\frac{d}{dX}\int_M^L dN\, N\exp[g(N) + N\mu] \approx \frac{d\mu}{dX}X_s^{(2)} \tag{32}$$

where the second equality applies for $X \approx X_{2c}$, where X_s approaches its saturation value (implying $g(N \leq L) \gg N|\mu|$) and long micelles just begin to appear in solution. The concentration of long micelles, though small, is already related to μ by eq 28. Hence, $X_l = X - X_s \approx X - X_s^{(1)} = \exp(-2\delta)/\mu^2$ from which we obtain $d\mu/dX = 1/2\exp(-\delta)(X - X_s^{(1)})^{-3/2}$. Using eqs 31 and 32, we find that for $X = X' \approx X_{2c}$

$$X' = X_s^{(1)} + \left(\frac{k}{2}\frac{X_s^{(2)}}{\exp(\delta)}\right)^{2/3} \tag{33}$$

This equation provides a relationship (accurate to leading order in $L\mu$) between the total concentration and the rate of change in X_s (as measured by $1/k$) in the "critical region". A well-defined second CMC implies that even a large change in k (e.g., from $k = 2$ to $k = 20$) should result in a very small change of X' in the vicinity of X_{2c}. This is only possible if two conditions are fulfilled. First, the second CMC is equal to the saturation concentration of small micelles

$$X_{2c} \equiv X_s^{(1)} = \exp(-2\delta)\int_M^L dN\, N\exp[g(N)] \tag{34}$$

Second, the inequality

$$[X_s^{(1)}]^3 \gg \left(\frac{k}{2}\frac{X_s^{(2)}}{\exp(\delta)}\right)^2 \tag{35}$$

must be satisfied for all (reasonably large) values of k. This latter condition ensures that the second CMC marks a sharp transition from small- to large-micelle populations. Insertion of the definition of the moments $X_s^{(m)}$ in eq 30 reveals that a necessary and sufficient condition for the fulfillment of the last inequality is that $g(N) \gg 1$ for at least some of the small- or intermediate-size micelles, $M \le N \le L$. For our model system, this condition is satisfied for $58 \le N \lesssim 70$ where $g(N) \approx 10$, see Figure 3.

Finally, we should verify that the approximation $L|\mu| \ll 1$ is indeed appropriate. From eq 33 and our previous result $X - X_s \approx X - X_s^{(1)} = \exp(-2\delta)/\mu^2$, we find $\mu(X = X_{2c}) = -[(2/k)\exp(-2\delta)/X_s^{(2)}]^{1/3}$. Thus, $L|\mu| \ll 1$ implies

$$L^3 \ll \frac{k}{2}\int_M^L dN\, N^2 \exp[g(N)] \tag{36}$$

For large values of k this inequality is trivially fulfilled, consistent with the fact that $k \to \infty$ implies $dX_s/dX \to 0$ and $X_1 \to X$, in which limit $\mu = -\exp(-\delta)/\sqrt{X} \to 0$. More significantly, the inequality will also be fulfilled for rather small k's (i.e., within the critical regime) provided for some small micelles $g(N) \gg 1$, which is exactly the condition ensuring the appearance of a sharp second CMC.

Concluding Remarks

Our molecular-level model of amphiphile packing in elongating linear micelles, albeit approximate, involves all of the important molecular and energetic characteristics of the constituent molecules. We have shown, for the first time (as far as we are aware of), that the interplay between inter-headgroup and interchain free energies plays a crucial role in determining the shapes and packing free energies of the growing micelles. For micelles composed of amphiphiles with strong propensity for cylindrical packing, we found that the final shape and energy of the endcaps is only established once the micelle's length is significantly larger than its diameter. The early stages of micellar elongation may involve a large energetic barrier, whose most apparent consequence is the lack of certain intermediate-size micelles from the micellar population and a typical second CMC behavior. We have also shown that the minimal micelles, likewise the endcaps of long micelles, are "bulkier" than the cylindrical body of the micelle. The conditions favoring the appearance of a second CMC have been characterized theoretically in terms of the molecular packing energies (micellar "standard chemical potential") and the thermodynamic formalism for micellar growth in dilute solution. Finally, our model calculations reveal all the essential growth characteristics of linear micelles, as observed in direct imaging experiments by Talmon and co-workers,[12,17] and somewhat less directly, yet most convincingly, by Porte and co-workers[11] and later by Kato et al.[13]

Acknowledgment. We thank Ishi Talmon and Anne Bernheim-Groswasser for most helpful discussions of their experimental results. The financial support of the Israel Science Foundation (Excellence Center grant No. 8003/97) and the US-Israel Binational Science Foundation (Grant No. 94/130) is gratefully acknowledged. The Fritz Haber research center is supported by the Minerva foundation, Munich, Germany. S.M. thanks the DFG for its support through SFB 197.

References and Notes

(1) Nusselder, J. J. H.; Engberts, J. B. F. N. *J. Org. Chem.* **1991**, *56*, 5522−5527.
(2) Gorski, N.; Kalus, J.; Meier, G.; Schwahn, D. *Langmuir* **1999**, *15*, 3476−3482.
(3) Taddei, G.; Amaral, L. Q. *J. Phys. Chem.* **1992**, *96*, 6102−6104.
(4) Romeu, N. V.; Taddei, G. *Colloid Polym. Sci.* **1999**, *277*, 1093−1097.
(5) McMullen, W. E.; Ben-Shaul, A.; Gelbart, W. M. *J. Coll. Int. Sci.* **1984**, *98*, 523−536.
(6) Ben-Shaul, A.; Gelbart, W. M. Statistical Thermodynamics of Amphiphile Self-Assembly: Structure and Phase Transitions in Micellar Solutions. In *Micelles, Membranes, Microemulsions, and Monolayers*, 1st ed.; Gelbart, W. M., Ben-Shaul, A., Roux, D., Eds.; Springer: New York, 1994.
(7) Israelachvili, J. N.; Mitchell, J.; Ninham, B. W. *J. Chem. Soc., Faraday Trans. 2* **1976**, *72*, 1525−1568.
(8) Israelachvili, J. N. *Intermolecular and Surface Forces*, 2nd ed.; Academic Press: London, 1992.
(9) Eriksson, J. C.; Ljunggren, S. *J. Chem. Soc., Faraday Trans. 2* **1985**, *81*, 1209−1242.
(10) Karaborni, S.; Esselink, K.; Hilbers, P. A. J.; Smit, B.; Karthäuser, J.; van Os, N. M.; Zana, R. *Science* **1994**, *266*, 254−256.
(11) Porte, G.; Poggi, Y.; Appell, J.; Maret, G. *J. Phys. Chem.* **1984**, *88*, 5713−5720.
(12) Bernheim-Groswasser, A.; Zana, R.; Talmon, Y. *J. Phys. Chem.* **2000**, *104*, 4005−4009.
(13) Kato, T.; Kanada, M. A.; Seimiya, T. *J. Coll. Int. Sci.* **1996**, *181*, 149−158.
(14) Tornblom, M.; Sitnikov, R.; Henriksson, U. *J. Phys. Chem. B* **2000**, *24*, 1529−1538.
(15) Zana, R.; Levy, H.; Danino, D.; Talmon, Y.; Kwetkat, K. *Langmuir* **1997**, *13*, 402−408.
(16) Ikeda, S.; Hayashi, S.; Imae, T. *J. Phys. Chem.* **1981**, *85*, 106−112.
(17) Bernheim-Groswasser, A.; Wachtel, E.; Talmon, Y. *Langmuir* **2000**, *16*, 4131−4140.
(18) Zheng, Y.; Won, Y.; Bates, F. S.; Davis, H. T.; Scriven, L. E.; Talmon, Y. *J. Phys. Chem. B* **1999**, *103*, 10 331−10 334.
(19) May, S.; Bohbot, Y.; Ben-Shaul, A. *J. Phys. Chem. B* **1997**, *101*, 8648−8657.
(20) May, S. *Eur. Biophys. J.* **2000**, *29*, 17−28.
(21) May, S.; Ben-Shaul, A. *Biophys. J.* **1999**, *76*, 751−767.
(22) Dan, N.; Pincus, P.; Safran, S. A. *Langmuir* **1993**, *9*, 2768−2771.
(23) Nielsen, C.; Goulian, M.; Andersen, O. S. *Biophys. J.* **1998**, *74*, 1966−1983.
(24) Harroun, T. A.; Heller, W. T.; Weiss, T. M.; Yang, L.; Huang, H. W. *Biophys. J.* **1999**, *76*, 3176−3185.
(25) Lundbæk, J. A.; Andersen, O. S. *Biophys. J* **1999**, *76*, 889−895.
(26) Fournier, J. B. *Europhys. Lett.* **1998**, *43*, 725−730.
(27) Evans, D. F.; Wennerström, H. *The Colloidal Domain, Where Physics, Chemistry, and Biology Meet*, 2nd ed.; VCH Publishers: New York, 1994.